Assessment of Global Numerical Weather Prediction Models for Short-term Solar Irradiation Forecasting in Southeastern South America

Vívian Teixeira-Branco[1], Rodrigo Alonso-Suárez[2] and Gabriel Cazes[3]

[1] Laboratorio Solar, ITR Centro-Sur, Universidad Tecnológica, Durazno (Uruguay)

[2] Laboratorio de Energía Solar, CENUR Litoral Norte, Udelar, Salto, Uruguay

[3] Facultad de Ingeniería, Universidad de la República, Montevideo (Uruguay)

Abstract

The accuracy of solar forecasts improves power system management, including energy dispatch and reserve handling. This work evaluates the performance of five numerical weather prediction models over southeastern South America over a three-year period. The first 24 hours of forecasts are analyzed at daily and hourly scales, taking into account seasonal and cloudiness discrimination. The models' performance shows little variation across geographical locations or seasons, and forecast accuracy deteriorates with increasing cloudiness. ECMWF shows the best performance with a daily rRMSD of 16.7%, despite underestimating solar radiation under clear skies. ICON follows with 18.0%, showing better behaviour under clear sky conditions. NEMS30 and GFS reach 21.0% and 21.9% respectively, with GFS underestimating cloudiness more and NEMS30 performing better under cloudy conditions. These results provide the first detailed evaluation of model performance in the region and highlight opportunities for improvement through post-processing techniques.

Keywords: Solar forecast, GHI, NWP, Global Models.

1. Introduction

Solar photovoltaic energy is the fastest growing energy source worldwide and is expected to remain the main driver of renewables in the coming years (IEA, 2025). Its intermittency, driven by the variability of the solar resource, poses new challenges to grid operators who need low uncertainty forecasts to balance supply and demand, manage dispatch and reserves, and support electricity market operations (Krishnan et al., 2023, Yang et al., 2020). Forecasting global horizontal irradiance (GHI) is a key factor for most solar PV forecasting systems. There are four main groups of solar forecasting methods, categorized according to the forecast horizon: all-sky cameras; satellite images; machine learning techniques or time series; and numerical weather prediction models (NWP). The application of these techniques, initially restricted to a specific temporal and spatial range, has undergone modifications in recent years due to advances in spatial and temporal resolution, mainly satellite and NWP, reducing the traditional separation between categories (Diagne et al., 2013; Inman et al., 2013; Yang et al., 2022). In terms of uncertainty, NWP offers good performance compared to other forecasting techniques for forecast horizons longer than 4-5 hours, extending up to days (Antonanzas et al., 2016; Diagne et al., 2013; Perez et al., 2013). These forecasting horizons are relevant for day-ahead and week-ahead grid planning and electricity markets.

NWP models are classified depending on their spatial scale as global or regional. Global models are only run by a few meteorological centers around the globe due to their high complexity and computational demands. Currently, there are 15 operational global models worldwide, and this number has not increased over the last decade (Diagne et al., 2014; Visser et al., 2022). The main differences between them are spatial resolution, vertical structure, and the physical schemes used to simulate atmospheric conditions. In contrast, regional models run over a limited spatial domain and therefore reduce computational requirements. In recent decades, several meteorological centers have developed their own regional models (WMO, 2020). This work evaluates the day-ahead (24-hour) performance of GHI forecasts from five global NWPs in southeastern South America. The selected models are widely used in the region: ECMWF, ICON and GFS at two spatial resolutions (0.25° and 0.50° equispaced in latitude and longitude). The evaluation also includes the NEMS30 model, which is of

local interest as it is used by the grid operator in Uruguay. The analysis is based on three consecutive years of forecasts, using as a reference controlled quality ground measurements distributed in the region and without applying any post-processing technique to the forecasts. The model performance is assessed over the whole period and by season, providing a fundamental step towards the robust development of improved solar forecasting tools in the region.

2. Data and Methods

2.1. Ground measurements

The reference observations are GHI measurements obtained at seven locations distributed throughout Uruguay, representative of the Humid Pampa subtropical region, belonging to the national solar monitoring network of the Solar Energy Laboratory (LES, http://les.edu.uy/). Stations are equipped with ISO 9060:2018 Class A pyranometers, calibrated biennially according to ISO-9847:1992 standards. The acquisition instruments record measurements at 1-minute intervals, from which hourly averages were calculated. Under optimal operating and maintenance conditions, the uncertainty assigned by the manufacturer to the equipment used is 2–3% on a daily basis. The measuring sites are presented in Table 1.

Table 1: Location of the ground measurement stations used in the work.

Site	Code	Lat. (deg)	Lon. (deg)	Alt. (m)
Salto	LE	− 31.28	− 57.92	42
Artigas	AR	−30.40	− 56.51	136
Tacuarembó	TA	−31.71	− 55.83	140
Canelones	LB	−34.67	− 56.34	32
Rocha	RC	−34.49	− 56.17	24
Colonia	ZU	−34.34	− 57.69	81
Treinta y Tres	PP	−33.26	− 54.49	58

2.2. Global Forecasting Models

The evaluated GHI forecasts come from five global NWPs: ECMWF, ICON, GFS at two resolutions (0.25° and 0.5°), and NEMS30, as shown in Table 2. ECMWF, also known as IFS, is developed by the European Centre for Medium-Range Weather Forecasts; GFS is produced by the National Center for Environmental Prediction (NCEP); ICON is part of the model suite of the German Weather Service (DWD, Deutscher Wetterdienst); and NEMS30 is a coupled weather model operated by the private company Meteoblue, configured to run over a global domain (Meteoblue, 2024).

Table 2: Configuration of the forecasting models used.

Characteristic	ECMWF	ICON	GFS 0.5°	GFS 0.25°	NEMS30
Spatial resolution	≈14 km	≈13 km	≈55 km	≈27 km	≈30 km
Vertical levels	137	90	64		60
Radiative transfer model	ecRad	RRTMG	RRTMG_SW (v2.3)		-
Prediction time step	1h	3h	3h		1h
Periods evaluated	2017-2019	2018-2020	2017-2019		2017-2019

All forecasts were initialized at 00 UTC. ECMWF and NEMS30 provide hourly GHI outputs, while ICON and GFS offer forecasts every three hours. The three-hour forecasts were interpolated following the methodology

of Verzijlbergh et al. (2015), using clear-sky irradiance estimates provided by the McClear model (Lefèvre et al., 2013). A three-hour clear-sky index was calculated from this information and used as the variable for linear interpolation to obtain hourly values. The hourly clear-sky index was then converted to hourly mean irradiance.

The forecast periods evaluated differ slightly among models, ranging mainly from 2017 to 2020; ICON is evaluated from 2018 to 2020, while the others are assessed from 2017 to 2019. The ICON and GFS models recently underwent updates to the radiative transfer scheme and the number of vertical levels, respectively, however, the evaluation period considered in this work does not include these updates.

2.3. Evaluation Metrics

The most common metrics used to quantify the performance of deterministic GHI forecasts are derived directly from the differences between ground-based observations and model predictions (Yang et al., 2018). The model's systematic bias is measured using the mean bias deviation (MBD), while dispersion is quantified using the mean absolute deviation (MAD) and the root mean square deviation (RMSD). The metrics area defined below:

$$MBD = \frac{1}{N}\sum_{i=1}^{N}\left(\hat{G}_h(i) - G_h(i)\right) \quad \text{(eq. 1)}$$

$$MAD = \frac{1}{N}\sum_{i=1}^{N}\left|\hat{G}_h(i) - G_h(i)\right| \quad \text{(eq. 2)}$$

$$RMSD = \sqrt{\frac{1}{N}\sum_{i=1}^{N}\left(\hat{G}_h(i) - G_h(i)\right)^2} \quad \text{(eq. 3)}$$

Relative values of these metrics are expressed as a percentage of the average ground-measured GHI. To evaluate the performance of a prediction model in relation to a reference model, the forecast skill (FS) is computed, which is defined as:

$$FS = 1 - \frac{RMSD_{forecast}}{RMSD_{persistence}} \quad \text{(eq. 4)}$$

A positive FS indicates that the forecast performs better than reference, while negative values denote poorer performance. In this study, the reference model is persistence. Persistence assumes that atmospheric conditions remain approximately stationary with respect to the previous time step. In this study, the hourly persistence model is obtained from the clear-sky index, which takes the same value hour by hour as on the previous day. On a daily scale, it is assumed that the daily clear-sky index remains constant from one day to the next.

In addition to metrics that quantify model uncertainty, categorical metrics are also used, such as the confusion matrix, to determine how many events (sky conditions) were correctly predicted by the models and how many were not. To evaluate the confusion matrix and estimate the models overall accuracy, the weighted balanced accuracy (BAW) was used, which is suitable for unbalanced data sets and defined as:

$$BAW = \frac{1}{N_p}\sum_g N_g\, BA_g \quad \text{(eq. 5)}$$

where N_g is the number of positive samples in class g and N_p is the total number of samples. Here, BA_g represents the balanced accuracy of each class, defined as the average of the true positive rate and the true negative rate for that class (Grandini et al., 2020). The classes considered here are clear sky, partly cloudy and overcast. These are defined by the clear-sky index (KC) thresholds set at KC > 0.90, 0.90 ≥ KC ≥ 0.40, and KC < 0.40, respectively.

3. Results

3.1. Intra-day forecast evaluation

Figure 1 plots performance metrics against the hourly forecast horizon (see the bottom *x* scale) or local time (see top *x* scale). The solid line represents the average performance across the evaluated sites, and the transparent area represents one standard deviation. In the intraday analysis, all models outperformed persistence. Over the annual period, the best performance was observed during midday hours. Among the

models, NEMS30 showed the largest intraday deviations, with rMBD values ranging from −7.1% to +27.1% and rRMSD between 30.2% and 50.5%. ECMWF showed the smallest deviations, with rMBD ranging from −3.0% to +3.5% and rRMSD between 23.6% and 32.4%. ICON achieved similar rRMSD values, ranging from 25.0% to 34.4%. For GFS-0.5, rRMSD ranged from 27.2% to 39.3%, and for GFS-0.25, from 28.4% to 39.1%.

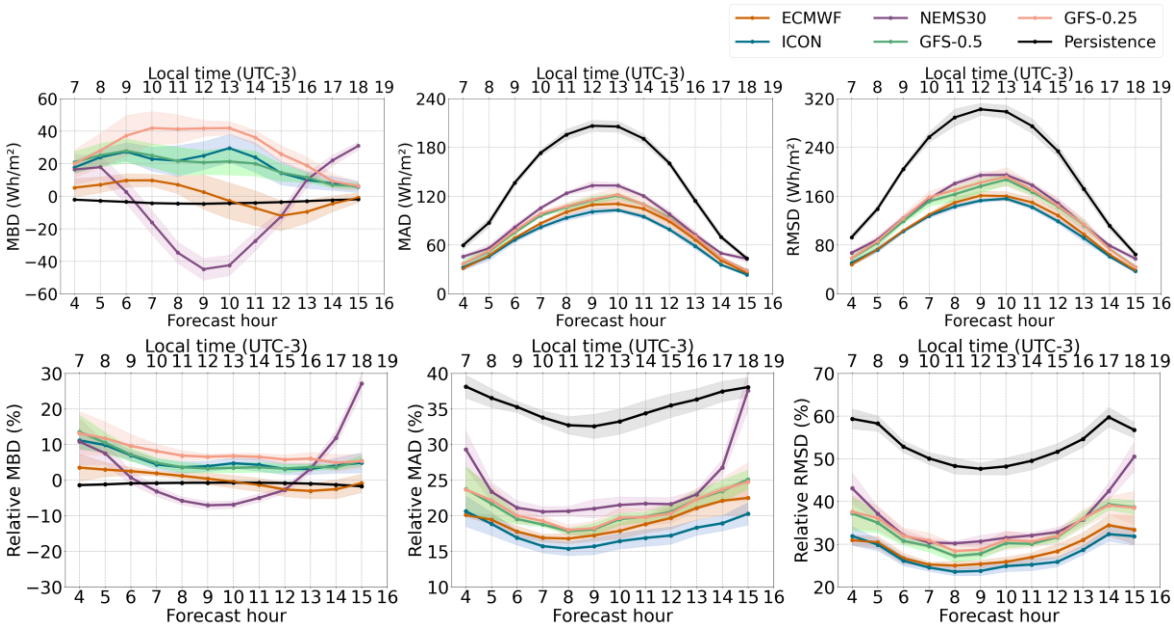

Figure 1: Intra-day performance metrics for day-ahead forecasts (MBD, MAD, RMSD), top: absolute values, bottom: relative values.

The forecast skill showed positive values throughout the day, as in Figure 2, due to the higher rRMSD values of the persistence model compared to the NWPs. NEMS30 shows the lowest performance, with FS values between 11.0% and 39.3%. ECMWF and ICON are the best performers of the models evaluated, with FS ranging from 41.2% to 49.6% and from 39.6% to 49.7%, respectively. The GFS–0.5 and GFS–0.25 models show intermediate performance, with values between 31.8% and 43.6% and between 32.1% and 41.2%, respectively.

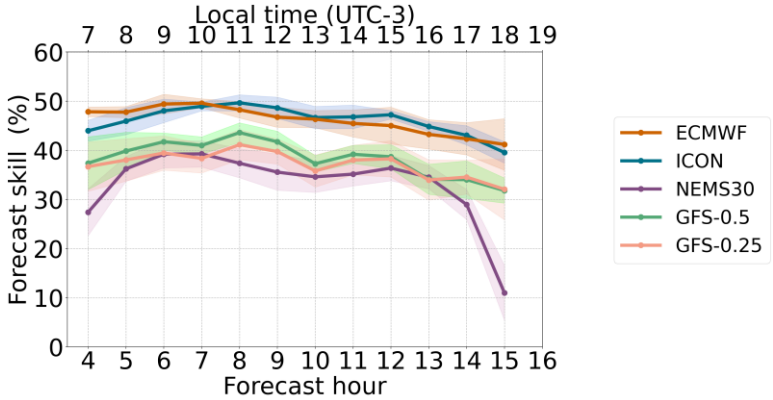

Figure 2: Intra-day FS from NWP models.

3.2. Daily forecast evaluation

The daily results correspond to the evaluation of the daily totals integrated in the first 24 hours of the forecast. Figure 3 shows the seasonal and annual relative RMSD at each site for the global models (bars) and for persistence (line). In the evaluation of the daily accumulated GHI, persistence was consistently outperformed by all models. From the performance comparison between persistence and global forecast models, it can be seen that the latter perform better in any period of the year, as expected. Persistence showed marked seasonal variability in the region, especially during winter and summer, with greater deviations compared to NWP models. This is evident when comparing the maximum seasonal standard deviation among models: for example, at the LB site, the NEMS30 model shows a standard deviation of around 3.4%, while persistence

reaches about 8.7% at PP. This characteristic seasonal behavior of persistence is novel in the region, as it had not been previously analyzed by Giacosa and Alonso-Suárez (2018). On the other hand, the individual analysis by site of the rRMSD for each model shows that the performance between sites is similar to each other, at any season of the year. The highest inter-site standard deviation was 2.9 % (≈ 0.5 MJ/m²), reported for GFS–0.25 during autumn. The average rMBD and rRMSD at the sites for each model during the evaluated periods are shown in Figure 4.

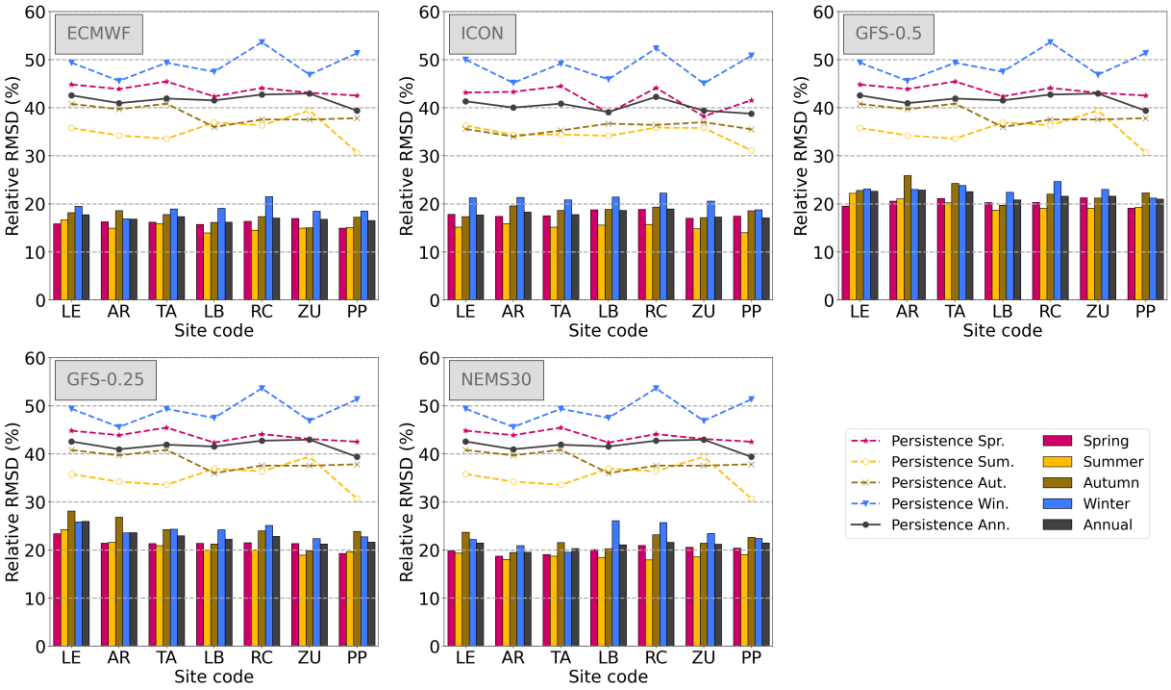

Figure 3: Daily relative RMSD for each model by site.

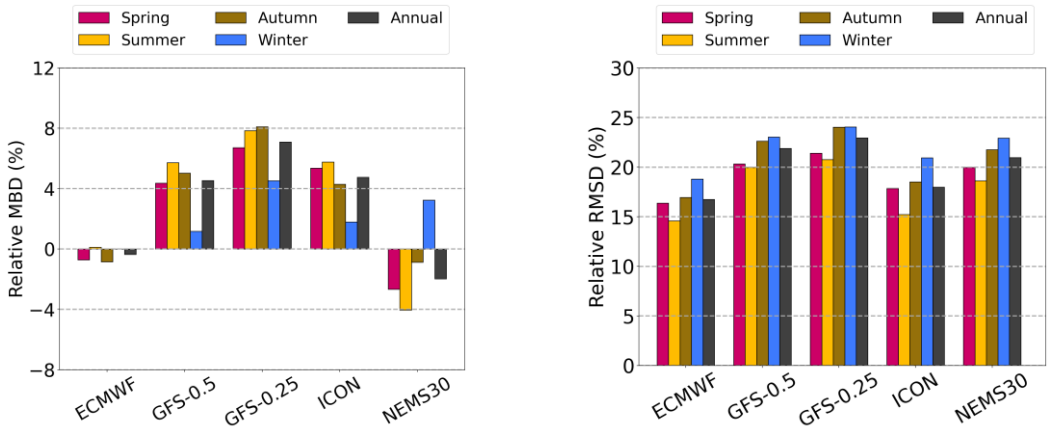

(a) Seasonal and annual daily relative MBD.

(b) Seasonal and annual daily relative RMSD.

Figure 4: Performance model daily forecast.

For the rRMSD (Figure 4b), the seasonal variability was smaller compared to the annual results, ranging from 1.7% to 2.8%. ICON and ECMWF had the lowest uncertainty, with annual rRMSD values of 18.0% and 16.7%, while GFS-0.25 had the highest at 23.0%. NEMS30 and GFS-0.5 performed intermediately with rRMSD values of 21.0% and 21.9%. In South America, the few studies available on the subject show that, as in other parts of the world, the performance of NWP models varies widely depending on the region and the forecast horizon. Lima et al. (2016) reported RMSD values between 20% and 67%, with high variability of the GFS+WRF model between the rainy and dry seasons in northeastern Brazil. In southeastern South America, Porrini (2017) highlighted the influence of the forecast horizon on model performance, with RMSD between 27% and 39% for GFS+WRF forecasts 1 to 3 days in advance. For this same region and time horizon, Teixeira-Branco et al. (2021) found rRMSD values between 25% and 32% for the ECMWF model. Figure 4 (a) shows

that the ECMWF and NEMS30 models tend to underestimate, with a maximum rMBD in autumn and a minimum in winter, with differences of approximately 0.8% and 3.1%, respectively. In contrast, models with an overestimation bias (ICON, GFS–0.5, and GFS–0.25) show a higher rMBD in summer and a lower one in winter, with seasonal differences of 4.5%, 3.3%, and 3.9%, respectively.

3.3. Dependence of forecast performance on sky conditions

The days were discriminated based on the clear sky index (KC). The three categories of sky conditions considered were: clear-sky (clc, KC > 0.90), partly cloudy (pcl, 0.90 ≥ KC ≥ 0.40), and cloudy or overcast (cld, KC < 0.40). No significant inter-site variability was found in the distribution of days among these categories. On average, across all sites, most days were classified as partly cloudy, followed by clear-sky and, to a lesser extent, cloudy. During the 2017-2019 period, clear days accounted for approximately 40% of the total, increasing slightly to 42% in the 2018-2020 period. Partly cloudy days accounted for 44% and 43% in the respective periods, while cloudy days accounted for around 16% and 15%.

Table 3 and Figure 5 show the seasonal evaluation of each sky condition for all models in terms of the average MBD across sites. Biases increase toward overestimation with greater cloudiness, regardless of model or season, suggesting that the annual (see Figure 4 a) overestimation arises mainly from unforecasted cloudy days. Under clear-sky conditions (Figure 5), all models show negative biases, particularly the ECMWF and NEMS30 models. The latter shows the greatest deviation under clear sky conditions, with MBD values between −0.3 MJ/m² and −1.9 MJ/m². During the summer and under cloudy conditions, the largest positive biases are observed, oscillating between +3.2 MJ/m² (NEMS30) and +7.5 MJ/m² (GFS–0.5), while ECMWF and ICON show intermediate values.

Table 3: Seasonal MBD based on sky conditions, in MJ/m^2

	ECMWF	ICON	GFS 0.5°	GFS 0.25°	NEMS30
Clear sky					
Spring	−1.5	−0.2	−0.6	−0.2	−1.6
Summer	−1.4	+0.2	−0.7	−0.1	−1.9
Autumn	−1.2	−0.5	−0.8	−0.3	−1.0
Winter	−0.9	−0.8	−0.7	−0.3	−0.3
Annual	−1.3	−0.3	−0.7	−0.2	−1.3
Partly cloudy					
Spring	+0.2	+1.8	+1.5	+2.0	−0.5
Summer	+0.7	+2.3	+2.2	+2.8	−0.9
Autumn	≈0.0	+0.9	+1.2	+1.6	≈0.0
Winter	+0.2	+0.4	+0.3	+0.6	+0.4
Annual	+0.3	+1.3	+1.3	+1.8	+0.2
Cloudy					
Spring	+2.9	+3.0	+3.0	+3.4	+2.2
Summer	+5.4	+3.7	+7.2	+7.5	+3.2
Autumn	+2.0	+2.4	+2.3	+2.7	+1.6
Winter	+1.4	+1.2	+1.0	+1.1	+1.3
Annual	+2.5	+2.3	+2.7	+3.0	+1.8

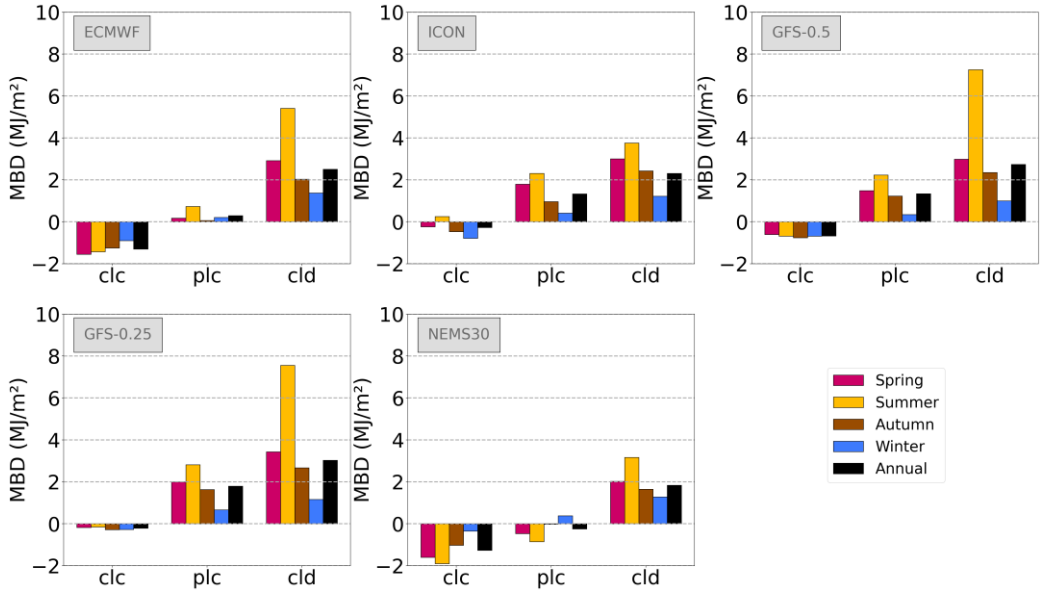

Figure 5: MBD for different sky conditions.

Table 4 and Figure 6 show the seasonal evaluation of each sky condition for all models in terms of the average RMSD across sites.

Table 4: Seasonal RMSD based on sky conditions, in MJ/m²

	ECMWF	ICON	GFS 0.5°	GFS 0.25°	NEMS30
Clear sky					
Spring	2.1	1.4	1.9	1.8	2.7
Summer	2.3	1.7	2.4	2.0	3.0
Autumn	1.9	1.2	1.6	1.4	2.0
Winter	1.3	1.1	1.1	0.9	1.2
Annual	2.0	1.4	1.9	1.6	2.4
Partly cloudy					
Spring	3.4	4.5	4.6	4.8	4.6
Summer	3.8	4.8	5.3	5.6	5.3
Autumn	2.4	2.9	3.5	3.7	3.5
Winter	1.9	2.2	2.5	2.7	2.6
Annual	3.0	3.7	4.1	4.4	4.1
Cloudy					
Spring	4.3	5.0	5.9	6.4	4.7
Summer	6.9	5.9	9.5	10.0	5.8
Autumn	3.1	4.0	4.3	4.7	3.4
Winter	2.2	2.6	2.9	3.0	2.6
Annual	4.0	4.2	5.4	5.8	4.0

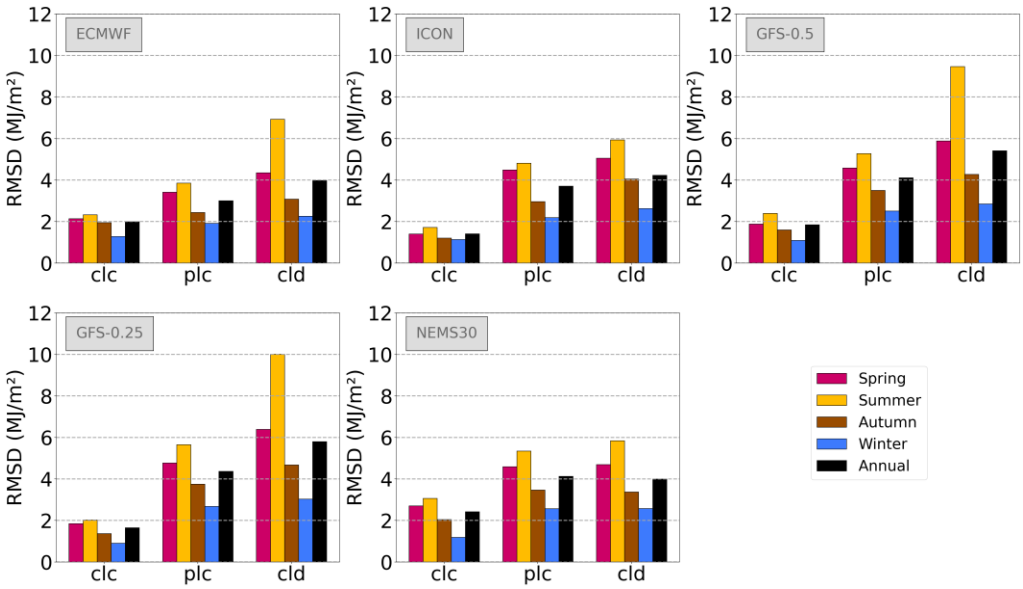

Figure 6: RMSD for different sky conditions.

Figure 6 shows that the performance of the forecast model decreases with increasing cloud cover, regardless of the season. For example, for the GFS–0.5, the RMSD is 1.9 MJ/m² under clear-sky conditions in spring, and increases to 5.9 (MJ/m²) on cloudy days. The highest RMSD values are observed in summer, especially on cloudy days, the GFS at different resolutions reaches approximately 10.0 MJ/m². The NEMS and ICON, and ECMWF excluding summer season, are the least affected models in this sense. GFS, on the other hand, shows the most affectation.

To complement the analysis, Figure 7 shows a more detailed evaluation of the relationship between RMSD and the clear sky index. The value represented on the x-axis corresponds to the center of a sample with ± 0.05 interval range. For example, at KC = 0.3, the values in the interval between KC > 0.25 and KC ≤ 0.35 are represented. Figure 7 shows that performance is similar at different periods of the year in most sky conditions, with a difference in KC < 0.2. In general, it is confirmed that in the region studied, seasonality has a low impact on the performance of GHI forecasting with global models. This was not observed in analysis by Lara-Fanego et al. (2012) for the region of Spain.

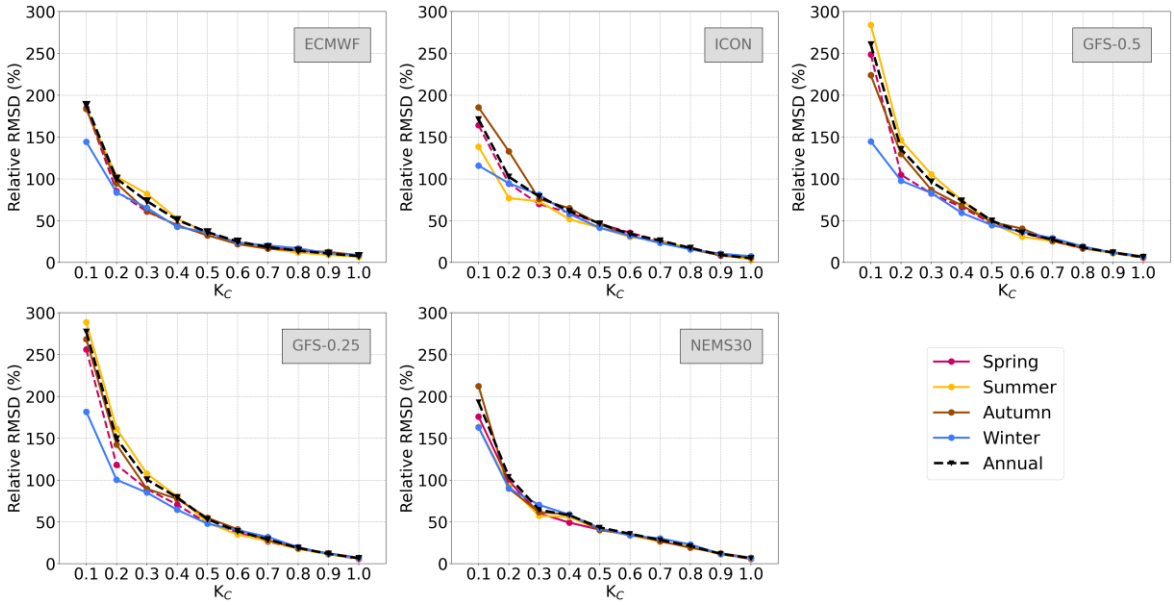

Figure 7: Annual and seasonal analysis of the average rRMSD between sites for different models based on the clear sky index.

Figure 8 shows a summary of the annual absolute and relative RMSD for all models as a function of the clear sky index. It can be seen forecast performance deteriorates with increasing cloudiness, especially for KC values below 0.5. GFS-0.5 and GFS-0.25 exhibit the highest uncertainty under cloudy conditions (KC = 0.1), with

RMSD values of 4.9 MJ/m² and 5.2 MJ/m², respectively. ICON, ECMWF, and NEMS30 show similar performance under these conditions. However, under clear-sky conditions (KC > 0.85), ECMWF presents RMSD values equal to or slightly higher than the other models, which is compensated by a better performance for 0.4 KC < 0.80.

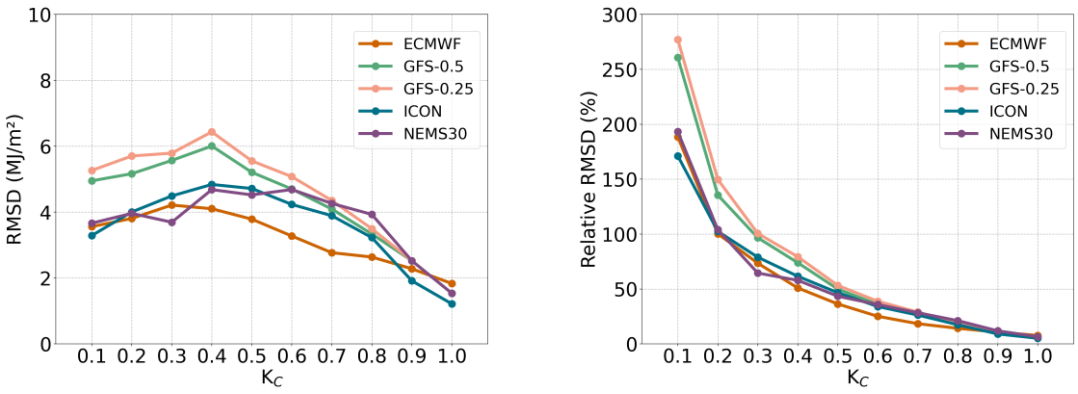

(a) KC vs. RMSD in absolute terms. **(b) KC vs. RMSD in relative terms.**

Figure 8: Annual analysis of the average rRMSD between sites for different models based on the clear sky index.

Another interesting analysis is presented in Figure 9. This figure presents the confusion matrix averaged across sites of the models' predicted sky classification through the KC thresholds in comparison with the same classification but using the ground measurements. The diagonal represents the correctly predicted sky conditions. The ECMWF model exhibits notable differences from the others, showing the lowest accuracy under clear-sky conditions (about 67.2%), while ICON performs best, with roughly 20% higher accuracy. Around 32.8% of clear-sky days are misclassified as partly cloudy by ECMWF, compared to only 12.8% for ICON. These results are consistent with the MBD analysis, which indicated ECMWF's tendency to underestimate solar irradiance on clear-sky days. Another characteristic that sets the ECMWF apart from other models is its high success rate under partly cloudy conditions, with 83.8% of predictions correct. In comparison, other models show values between 54.1% (GFS–0.25) and 65.2% (ICON).

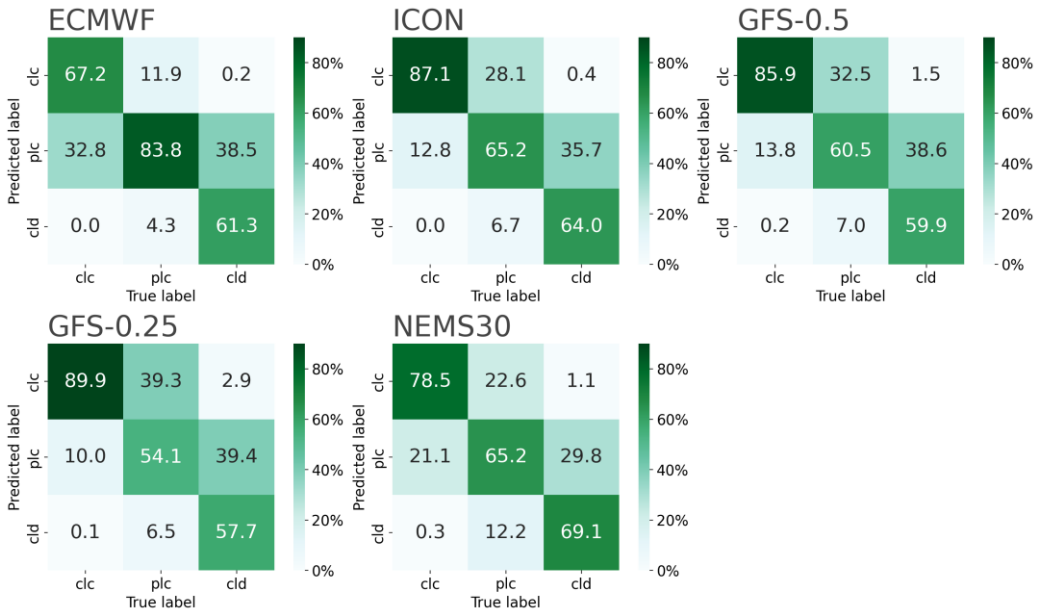

Figure 9: Confusion matrix averaged across sites for each model.

In the cloudy sky category, NWP models show similar accuracy rates, ranging from 57.7% (GFS–0.25) to 69.1% (NEMS30). Most errors correspond to cloudy days misclassified as partly cloudy, revealing the models' weakness in predicting high cloud cover conditions. In contrast, models infrequently confuse clear-sky days with cloudy days, indicating that they have difficulty distinguishing between adjacent classes but can clearly distinguish between opposite ones. It should be noted that it is unknown whether the improvement in

NEMS30's performance in such complex conditions is due to any post-processing applied by the proprietary company. In terms of overall balanced accuracy weighted, the ECMWF model has superior ability to predict different categories of sky conditions, with a BAW of 76.0%. Next are the ICON (74.0%), NEMS30 (71.0%), GFS–0.5 (71.0%), and GFS–0.25 (69.0%) models.

4. Conclusions

This work represents the first comprehensive performance assessment of GHI forecasts provided by different global numerical weather models in the southeastern region of South America on an intra-day and daily scale. The evaluation of the forecast models included analysis of annual and seasonal performance based on several metrics that are widely used in the area (MBD, MAD, RMSD, and FS), as well as analysis of prediction quality in conceptual sky categories (BAW). It also presented the information with useful visual diagrams, such as performance discrimination based on different sky conditions. The predictions significantly surpassed the performance of the persistence forecast on all of the time scales evaluated. The models evaluated showed no significant geographical or seasonal dependence, with low performance variability throughout the year.

On an intra-day scale, the best performance was recorded during the middle of the day. The ECMWF model showed the lowest uncertainty (rRMSD between 23.6% and 32.4%), while NEMS30 showed the highest intra-day variability (rRMSD between 30.2% and 50.5%). ICON showed slightly higher values (rRMSD between 25.0% and 34.4%), whereas GFS–0.5 and GFS–0.25 ranged between 27.2–39.3% and 28.4–39.1%, respectively. In terms of daily integrated values, ECMWF achieved the best overall results (rRMSD ≈ 16.7%), although it tends to underestimate the clear-sky solar irradiance; ICON showed a comparable behavior, with slightly higher uncertainty (rRMSD ≈ 18.0%). GFS-0.5 performed acceptably, but exhibited greater uncertainty under cloudy conditions (rRMSD ≈ 21.9%). The NEMS30 showed marginally lower performance (rRMSD ≈ 21.0%), but competitive results on cloudy days, possibly due to the use of proprietary post-processing by the operating company. Future work will focus on reducing forecast uncertainty through post-processing and developing probabilistic solar forecasts up to five days ahead, an area not yet explored in the region.

5. References

Antonanzas, J., Osorio, N., Escobar, R., Urraca, R., Martinez-de-Pison, F. J., & Antonanzas-Torres, F., 2016. Review of photovoltaic power forecasting. Solar Energy, 136, 78-111.

Diagne, M., David, M., Boland, J., Schmutz, N., & Lauret, P., 2014. Postprocessing of solar irradiance forecasts from WRF model at reunion island. Energy Procedia, 57, 1364-1373.

Diagne, M., David, M., Lauret, P., Boland, J., & Schmutz, N., 2013. Review of solar irradiance forecasting methods and a proposition for small-scale insular grids. Renewable and Sustainable Energy Reviews, 27, 65-76.

Giacosa, G., & Alonso-Suárez, R., 2018. Desempeño de la persistencia para la predicción del recurso solar en Uruguay. Revista Brasileira de Energía Solar 9(2):107-116, 2018.

Grandini, M., Bagli, E., & Visani, G., 2020. Metrics for Multi-Class Classification: an Overview. https://arxiv.org/abs/2008.05756

IEA, 2025. Renewables 2025. Technical Report. International Energy Agency.

Inman, R. H., Pedro, H. T., & Coimbra, C. F., 2013. Solar forecasting methods for renewable energy integration. Progress in Energy and Combustion Science, 39(6), 535-576.

Krishnan, N., Kumar, K.R., Inda, C.S., 2023. How solar radiation forecasting impacts the utilization of solar energy: A critical review. Journal of Cleaner Production 388, 135860.

Lara-Fanego, V., Ruiz-Arias, J., Pozo-Vázquez, D., Santos-Alamillos, F., & Tovar Pescador, J., 2012. Evaluation of the WRF model solar irradiance forecasts in Andalusia (southern Spain). Solar Energy, 86, 2200-2217.

Lefèvre et al., 2013. Mcclear: a new model estimating downwelling solar radiation at ground level in clear-sky conditions. Atmospheric Measurement Techniques 6, 2403–2418.

Lima, F.J., Martins, F.R., Pereira, E.B., Lorenz, E., Heinemann, D., 2016. Forecast for surface solar irradiance at the brazilian northeastern region using NWP model and artificial neural networks. Renewable Energy 87, 807–818.

Meteoblue. (2024). Datasets. Retrieved from https://docs.meteoblue.com/en/meteo/data-sources/datasets#nems.

Perez, R., Lorenz, E., Pelland, S., Beauharnois, M., Van Knowe, G., Hemker, K., Heinemann, D., Remund, J., Müller, S. C., Traunmüller, W., Steinmauer, G., Pozo, D., Ruiz-Arias, J. A., Lara-Fanego, V., Ramirez-Santigosa, L., Gaston-Romero, M., & Pomares, L. M., 2013. Comparison of numerical weather prediction solar irradiance forecasts in the US, Canada and Europe. Solar Energy, 94, 305-326.

Porrini, C., 2017. Evaluación del modelo regional WRF para pronósticos de radiación solar en superficie dentro del territorio uruguayo.

Teixeira-Branco, V., Alonso-Suárez, R., & David, M. (2021). Performance assessment of the ECMWF solar irradiation forecast in the Pampa Húmeda region of South America. Proceedings of the ISES Solar World Congress.

Verzijlbergh, R. A., Heijnen, P. W., R., S., Los, A., & Jonker, H. J., 2015. Improved model output statistics of numerical weather prediction based irradiance forecasts for solar power applications. Solar Energy, 118, 634-645.

Visser, L., Lorenz, E., Heinemann, D., & van Sark, W. G., 2022. Solar Power Forecasts. In Comprehensive Renewable Energy (Second Edition, pp. 213-233). Elsevier.

Yang, D., Kleissl, J., Gueymard, C.A., Pedro, H.T., Coimbra, C.F., 2018. History and trends in solar irradiance and PV power forecasting: A preliminary assessment and review using text mining. Solar Energy 168, 60–101.

Yang et al., 2020. Verification of deterministic solar forecasts. Solar Energy 210, 20–37.

Yang, D., Wang, W., Gueymard, C. A., Hong, T., Kleissl, J., Huang, J., Perez, M. J., Perez, R., Bright, J. M., Xia, X., van der Meer, D., & Peters, I. M., 2022. A review of solar forecasting, its dependence on atmospheric sciences and implications for grid integration: Towards carbon neutrality. Renewable and Sustainable Energy Reviews, 161, 112348.